Research Square

Preprints are preliminary reports that have not undergone peer review.
They should not be considered conclusive, used to inform clinical practice,
or referenced by the media as validated information.

Productivity and surface-texture trade-offs in jet-electrodeposited copper tracks: a replicated factorial study

Thiago Ferreira Querino

tquerino@ufu.br

UFU: Universidade Federal de Uberlandia https://orcid.org/0009-0000-5709-5627

Letícia Bueno do Amaral

Rafaela Evangelista da Silva

Arthur Alves Fiocchi

UFU: Universidade Federal de Uberlandia

Research Article

Keywords: Electrochemical additive manufacturing, Pareto dominance, Profile waviness, Nozzle scanning speed, Volumetric metrology, Galvanostatic control

Posted Date: November 24th, 2026

DOI: https://doi.org/10.21203/rs.3.rs-11543193/v1

License: This work is licensed under a Creative Commons Attribution 4.0 International License.
Read Full License

Productivity and surface-texture trade-offs in jet-electrodeposited copper tracks: a replicated factorial study

Thiago Ferreira Querino*, Letícia Bueno do Amaral, Rafaela Evangelista da Silva, Arthur Alves Fiocchi

*E-mail address of Corresponding author: tquerino@ufu.br

Abstract: *Jet electrodeposition offers localized, low-temperature fabrication of metallic features, but selecting operating conditions requires balancing deposition productivity, geometrical development, surface texture, and repeatability. This study investigates the combined effects of applied current (2–6 mA) and nozzle scanning speed (0.6–1.4 mm/min) on single-pass copper tracks fabricated on copper substrates. A replicated 5 × 5 full-factorial design (125 trials) was evaluated using volume-derived apparent material deposition rate (MDR), maximum track height (H_{max}), profile roughness (Ra), and waviness (Wa). Factorial analysis of variance, variability metrics, and an experimental three-objective Pareto classification were employed; quadratic response surfaces were also assessed for model adequacy. Mean MDR increased from 0.017 to 0.058 mg/min between the lowest and highest scanning speeds, although this change was strongly influenced by deposition-time normalization. The highest MDR (0.08845 mg/min; 6 mA, 1.4 mm/min) exhibited substantially greater variability than a lower-throughput alternative at 5 mA and the same speed. Maximum track height ranged from 8.955 to 15.923 µm and was weakly correlated with MDR (r = 0.122). Minimum Ra (0.673 µm) and Wa (1.133 µm) occurred at different current–speed settings, with significant interactions between the processing factors for both texture responses. Ten of the 25 conditions were non-dominated when maximizing MDR while minimizing Ra and Wa. Because the quadratic models exhibited significant lack of fit, recommendations were confined to experimentally tested combinations. These findings establish an application-oriented framework for identifying transparent productivity–quality trade-offs in localized copper manufacturing.*

Keywords: *Electrochemical additive manufacturing; Pareto dominance; Profile waviness; Nozzle scanning speed; Volumetric metrology; Galvanostatic control.*

1. INTRODUCTION

Metal additive manufacturing (MAM) has become an established route for producing geometrically complex and application-specific components through controlled material addition. Current metal AM families include powder-bed fusion, directed energy deposition, binder jetting, and related processes, each providing distinct combinations of geometric freedom, material compatibility, productivity, and dimensional accuracy [1]. These approaches are increasingly applied to aerospace and biomedical components, tooling, and functional metallic structures. Nevertheless, translating their capabilities to micro- and mesoscale features remains challenging: fusion-based processes may

introduce heat-affected microstructures, thermal stresses, porosity, and relatively rough surfaces, whereas powder-based routes often require substantial post-processing. As feature dimensions decrease, local control of material addition and the repeatability of surface and dimensional quality become as important as the ability to fabricate complex shapes [1, 2].

Electrochemical additive manufacturing (ECAM) offers a complementary, predominantly non-thermal approach in which metal ions are reduced at selected locations of an electrically conductive surface. By controlling the electrochemical reaction zone, ECAM can fabricate micro- and nanoscale metallic structures without melting a bulk feedstock and with potential applications in microelectronics, sensors, robotics, and energy-storage devices [3]. Ayalew et al. [2] identified maskless localized deposition as a promising alternative to lithography-dependent electroforming for complex small features. However, electrochemical printing is not a single manufacturing process: meniscus-confined electrodeposition, probe-based localized deposition, and jet-assisted configurations differ markedly in liquid confinement, ion replenishment, throughput, and the achievable feature dimensions. A recent critical review emphasized that deposition kinetics, surface morphology, and process stability remain closely coupled, complicating the transfer of optimized conditions between ECAM platforms [4].

Within this group, jet electrodeposition (Jet ECD) employs a flowing electrolyte column to provide an ionic connection between the anodic region and a localized cathodic deposition zone. Continuous electrolyte renewal can mitigate local depletion of electroactive species and enables maskless manufacturing through programmed nozzle motion. This architecture is attractive for conductive tracks, localized metallic coatings, microelectrodes, and more complex copper structures. Nevertheless, it introduces a coupled multiphysics problem: the nozzle trajectory and local exposure time interact with current distribution, effective electrode separation, electrolyte transport, and the moving deposition front. In comparison with meniscus-based techniques, free-flow jets may facilitate faster deposition, but lateral spreading and nonuniform growth can compromise geometric localization and surface consistency [5, 6, 7].

Experimental studies demonstrate both the technological promise and the diversity of performance metrics used in Jet ECD. Arshad et al. [6] obtained localized copper deposits on stainless steel with a reported minimum surface roughness of 0.38 ± 0.02 μm at a material deposition rate of 16.06 μg/s; under the authors' process conditions, the reported rate was approximately 20 times that of a meniscus-confined approach. Ye et al. [8]

fabricated copper microcolumns approximately 70 μm in diameter at a reported axial growth rate of 19.8 μm/s after optimizing electrolyte composition and voltage. Gu et al. [9] developed a circulating electrolyte-jet printer that achieved a reported copper growth rate of 53.4 μm/h, an atomic-force-microscopy (AFM) roughness as low as Ra = 1.1 nm, and microhardness up to 3.3 GPa. These achievements concern different geometries, deposition modes, and characterization scales: axial growth rates in μm/s or μm/h, mass-based rates in μg/s, and roughness measured over nanometric AFM fields cannot be directly ranked against full-track volume-derived MDR or millimetre-length profile roughness.

Surface integrity and spatial localization remain particularly sensitive to the hydrodynamic boundary conditions. Li et al. [10] changed the aspect ratio of rectangular nozzles during copper Jet ECD and reported that areal roughness Sa decreased from 5.40 to 2.76 μm, a reduction of approximately 48.9 %; the least favorable configuration produced a deposition footprint equivalent to 192 % of nozzle width. Their observations linked a more uniform flow field to fewer nodular deposits and improved localization. More recently, Dong et al. [11] combined electrolyte-additive investigations, Taguchi experiments, response-surface optimization, and cathode pretreatment to produce copper columns with Sa near 65 nm and increase initial-stage deposition efficiency by more than 50 %; their printed planar structures exhibited an average Sa of approximately 0.20 μm. Although these studies provide compelling examples of process optimization, their reported Sa values describe areal topography and should not be interpreted as directly equivalent to longitudinal profile Ra or Wa obtained under different filtering and evaluation conditions.

The need to coordinate metal growth with nozzle motion becomes even more evident in three-dimensional Jet ECD. Rajput et al. [5] formulated and experimentally examined a physics-based model for selective jet deposition, linking applied voltage, metal-ion concentration, and interelectrode gap to predicted deposition rate and height. Kamaraj and Sundaram [12] subsequently developed a model incorporating electrical processing conditions and horizontal scanning speed to predict deposition rate and layer height. More recent feedback strategies address behavior that cannot be adequately represented by a simple fixed-rate assumption: Xiang et al. [7] demonstrated automated copper structures with unsupported overhangs up to 80 °, 98.5 wt% of copper purity, and a reported local Ra of 18.54 nm using image recognition and voltage feedback. The same study reported nonlinear changes in deposition rate as geometry evolved, highlighting the need to

distinguish mechanistic or feedback-based prediction from low-order empirical interpolation.

Despite these advances, important gaps remain for the manufacturing of single-pass copper tracks. Much of the available literature emphasizes deposition rate, feature height or width, areal roughness, and the demonstration of geometrically complex structures, while quantitative assessment of longitudinal waviness and its relation to process-parameter interactions and between-track repeatability is less prominent in the studies surveyed [6, 10, 9, 11]. This distinction is relevant because roughness and waviness describe different spatial bands of surface variation; neither parameter alone establishes the mechanisms responsible for the observed texture. In addition, a high reported deposition rate may reflect the chosen time or area normalization and does not necessarily imply a greater deposited mass, a larger feature height, or more repeatable production. For a balanced selection of manufacturing conditions, productivity, geometry, profile texture, and experimental variability therefore need to be evaluated jointly. Whether a simple response-surface model can interpolate these responses reliably must also be tested, rather than presumed from the availability of a factorial dataset.

Against this background, the present study examines a previously generated, replicated Jet ECD dataset for single-pass copper tracks on copper substrates [13]. A full 5 × 5 factorial arrangement combines applied current (2–6 mA) and nozzle scanning speed (0.6–1.4 mm/min), with five independent tracks per condition (125 trials). The objectives are to (i) quantify apparent, volume-derived material deposition rate (*MDR*) and its repeatability; (ii) determine the separate and interacting effects of current and speed on maximum track height ($H_{máx.}$), longitudinal roughness (*Ra*), and waviness (*Wa*); and (iii) identify experimentally non-dominated operating conditions by maximizing MDR while minimizing *Ra* and *Wa*. Quadratic response surfaces are evaluated as exploratory interpolation tools and are subjected to model-adequacy tests before any optimization claim. The resulting analysis aims to provide a transparent, application-oriented interpretation of process trade-offs within the tested domain, without claiming that a single operating condition optimizes every functional requirement.

2. MATERIALS AND METHODS

2.1. Jet ECD experimental setup

Experiments were conducted using a multifunctional miniature machine-tool platform developed at the the FEMEC MAKER Advanced Manufacturing Laboratory, Federal University of Uberlândia (UFU), Brazil. The system architecture was based on the approaches reported by Ye, Niu, and Wang [8] and the apparatus described by Amaral [13]. Figure 1 schematically illustrates the Jet ECD setup integrated into the additive manufacturing platform.

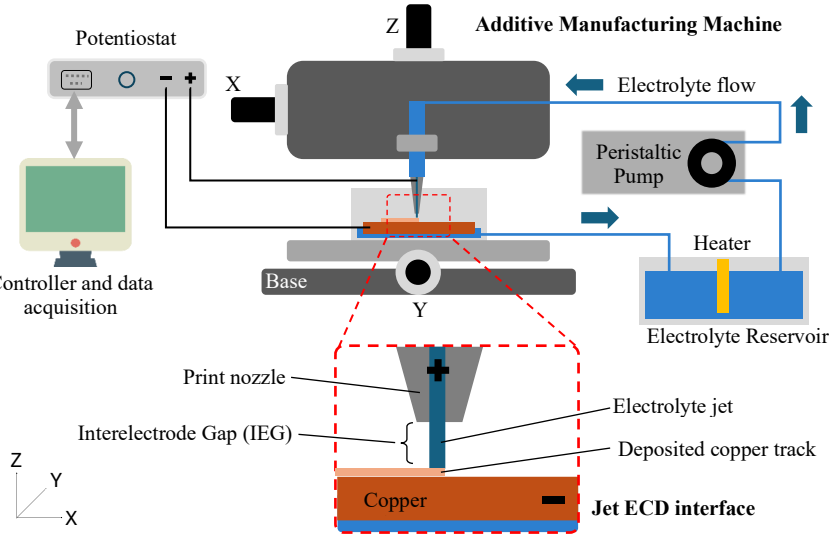

Figure 1 - Schematic of the Jet ECD apparatus integrated into the additive manufacturing platform.

The computer-controlled platform coordinated the imposed electrodeposition current and nozzle motion to fabricate single-pass copper tracks 6.0 mm in length. The exposed end of the copper anode was coplanar with the syringe outlet; therefore, the initial nozzle-to-substrate clearance corresponded to the nominal interelectrode gap (IEG). This initial gap was set to 0.50 mm using a feeler gauge of the same thickness. The electrolyte was delivered by a peristaltic pump while the nozzle translated along the X axis. Electrical connection to the anode was provided through a terminal-block connector, whereas the copper substrate served as the cathode through a conductive contact in the glass cell. Galvanostatic deposition was initiated after establishing the electrolyte jet. The stated IEG represents the initial geometric setting and does not imply that the effective electrode separation remained unchanged as the copper deposit grew.

An Ivium Vertex potentiostat (Ivium Technologies, the Netherlands) was operated in galvanostatic chronopotentiometric mode. Constant electrodeposition currents ranging from 2 to 6 mA were imposed according to the experimental design.

The electrolyte was supplied by a custom-built peristaltic pump developed at FEMEC MAKER. A pulse-controlled drive regulated the pump-rotor speed and enabled

nominal flow-rate adjustment over 0.27–2.50 mL/s. According to the original experimental procedure, flow rate was calibrated by recording the time needed to fill a 100 mL graduated vessel at the selected pump setting. The nominal electrolyte flow rate was fixed at 2.50 mL/s for the experiments considered here.

The deposition module comprised a modified 1 mL syringe coupled to the peristaltic-pump tubing by a photopolymerization-based additively manufactured adapter. The syringe outlet had a nominal diameter of approximately 0.50 mm.

Copper substrates were mounted in a glass cell using an internal support grid and fused-filament-fabricated poly(lactic acid) (PLA) clamps. Electrical contact was established by a conductive wire held against the substrate by the clamping assembly.

The electrolyte reservoir was equipped with a 25 W submersible heater (H-386, Hopar Aquarium Heater). The nominal electrolyte temperature for the experimental campaign was 35 °C.

2.2. Materials and deposition conditions

The electrolyte was prepared by dissolving copper(II) sulfate pentahydrate ($CuSO_4 \cdot 5H_2O$; 0.96 mol/L), sulfuric acid (H_2SO_4; 0.76 mol/L), hydrochloric acid (HCl; 0.0016 mol/L), and sodium saccharin dihydrate ($C_7H_4NNaO_3S \cdot 2H_2O$; 0.0015 mol/L) in distilled and deionized water.

Commercial copper plates measuring 15 × 15 × 2 mm, originally intended as heat spreaders in electronic assemblies, were used as conductive substrates.

Prior to electrodeposition, the copper substrates were sequentially wet-ground using abrasive papers of grit sizes 900, 1200, and 2000 on a glass support. The substrates were then rinsed with running water, cleaned with isopropyl alcohol (≥99.8%), and ultrasonicated at 40 kHz for 10 min in distilled water containing 10 % (v/v) neutral detergent. Subsequently, surface activation was performed using an acidified solution consisting of 5 % of acetic acid (commercial vinegar) and sodium chloride (NaCl), in a ratio of 5 g of NaCl per 100 mL of diluted acetic acid. The substrate was immersed in the solution for 3 minutes, with light, intermittent agitation to ensure uniform contact with the surface. For drying and storage, the samples were dried using lint-free absorbent paper and then stored in polypropylene boxes under ambient atmospheric conditions until the time of electrodeposition.

2.3. Experimental design

A 5 × 5 full-factorial experimental design was adopted to investigate applied electric current (2, 3, 4, 5, and 6 mA) and nozzle scanning speed (0.6, 0.8, 1.0, 1.2, and 1.4 mm/min). Single-pass copper tracks with a nominal deposition length of 6.0 mm were manufactured. Five replicate specimens were assigned to each parameter combination, resulting in 125 experimental trials. The experimental factors, fixed conditions, and measured responses are summarized in Table 1.

Table 1 - Experimental factors, fixed processing conditions, and response variables

Input parameters (variables)	Input parameters (constants)	Output parameters (to be analyzed)
Applied electric current (i): 2, 3, 4, 5, and 6 mA **Nozzle scanning speed (v): 0.6, 0.8, 1.0, 1.2, and 1.4 mm/min**	Electrolyte composition: 0.96 mol/L $CuSO_4 \cdot 5H_2O$; 0.76 mol/L (H_2SO_4); 0.0016 mol/L HCl and 0.0015 mol/L sodium saccharin IEG : 0.5 mm Electrolyte flow rate: 2.50 mL/s Copper substrate Electrolyte temperature: 35 °C	Apparent MDR and CV Maximum track height (Hmax) Profile Ra, Rq and Wa, Wt Between-track dispersion (SD, CV)

2.4. Geometrical and Surface-Texture Characterization

The topography of the electrodeposited copper tracks was acquired using a UBM Microfocus Expert IV laser optical profilometer at the Laboratory of Tribology and Materials (LTM), UFU. Each scan covered a nominal surface area of 1.5 × 7.0 mm², comprising the 6.0 mm track and adjacent substrate regions. The original measurement record reports a nominal 1,000 × 1,000-point acquisition grid and instrumental lateral and vertical resolution specifications of 0.1 μm and 60 nm, respectively. These nominal resolution figures were not interpreted as the effective spacing of the acquired points or as a calibrated measurement uncertainty.

Topographic datasets were processed in MountainsMap software (version 11.0, Digital Surf, Besançon, France). The software was used to analyze the three-dimensional surface, extract longitudinal track profiles, determine track height and geometric volume,

and calculate profile roughness and waviness parameters. The processing workflow included geometrical leveling, form removal, feature segmentation, and profile filtering, as specified below.

For volume assessment, the measured topography was leveled by least-squares plane (LSPL) fitting, followed by third-order polynomial form removal. The MountainsMap Slice tool was then used to delimit the copper track relative to the surrounding substrate by adjusting a virtual height-sectioning plane until the deposited feature could be distinguished in the topographic map. The volume assigned to the segmented deposit was obtained from the three-dimensional surface data within the acquired field, rather than by extrapolating a two-dimensional profile across an assumed track width. Because selection of the sectioning threshold involves operator judgment, the resulting volumetric estimate is treated as an apparent geometrical quantity; an independent sensitivity analysis of the segmentation level was not available.

The deposited copper mass was estimated from the measured track volume using the nominal density of copper (ρ = 8.96 g/cm³), assuming bulk-equivalent copper density; porosity or oxide inclusions were not independently corrected. The apparent material deposition rate (*MDR*) was calculated as the estimated mass divided by the deposition time (t, min), as shown in Eq. (1). With V expressed in cm³ and ρ in g/cm³, the conversion factor 10^3 yields *MDR* in mg/min.

$$MDR = \frac{\rho \cdot V}{t} \times 10^3 \quad (1)$$

All volume-derived results were retained, including conditions for which the estimated *MDR* exceeded the theoretical Faradaic deposition-rate limit. Such discrepancies were not interpreted as current efficiencies greater than 100 %, since the calculated *MDR* represents a geometrically inferred quantity rather than a direct gravimetric measurement. Potential differences between the apparent and theoretical deposition rates may arise from uncertainties associated with the topographic reference surface, volume integration, and the assumption of bulk-equivalent deposit density.

Longitudinal profiles were extracted along the nominal centerline of the deposited copper tracks. A central evaluation length of 4.0 mm was used, excluding approximately 1.0 mm at each end of the nominally 6.0 mm track to reduce end-of-track effects. Before

profile-parameter calculation, the measured data were subjected to LSPL leveling and third-order polynomial form removal. This distinction between geometrical form removal and subsequent wavelength-selective filtering was preserved during interpretation of surface texture.

Filter settings were selected with reference to ISO 21920-2:2021 and ISO 21920-3:2021 [14, 15], using Setting Class 3 (Sc_3) as a criterion for choosing the profile-processing parameters, rather than as a claim of full metrological conformity. The selected processing indices were 2.5 μm for the initial small-scale profile *S*-filter, 0.8 mm for the roughness-profile *L*-filter, and 0.8 mm for the waviness-profile *S*-filter used to separate shorter-wavelength texture from longer-wavelength components. Roughness parameter *Ra* were calculated from the corresponding *R*-profiles, whereas waviness parameter *Wa* were obtained from *W*-profiles over the 4.0 mm evaluation length. The same nominal settings were applied to all experimental conditions to support within-dataset comparison. The stated settings do not, by themselves, establish conformity of the original spatial sampling or instrument calibration with every requirement of the referenced standard.

Maximum track height ($H_{máx.}$) was treated as a distinct geometrical descriptor obtained from the longitudinal track-profile assessment after geometrical leveling. It was not inferred from *Ra* or *Wa*, which characterize filtered profile-texture components. No certified measurement uncertainty or independently verified correction for unmeasured points was available for this retrospective analysis.

2.5. Statistical analysis

For each current–speed combination, results from five nominally independent tracks were summarized using the arithmetic mean and sample standard deviation (*sd*). Relative dispersion was described by the coefficient of variation, $CV = 100 \times sd/mean$, for nonzero means. Balanced two-way fixed-factor analysis of variance (ANOVA) was used to investigate *MDR*, H_{max}, *Ra*, and *Wa*, including the effects of applied current (five levels), scanning speed (five levels), and their interaction, with a significance threshold of $\alpha = 0.05$. Where only condition summaries were available, ANOVA sums of squares and pure-error terms were reconstructed from the 25 condition means, *sd's*, and $n = 5$ replicates per combination; partial eta-squared was reported as an effect-size indicator. *MDR* residual normality was assessed using the Shapiro–Wilk test, and heteroscedasticity-consistent HC_3 inference was used as a sensitivity analysis for the *MDR* model. Conventional

ANOVA p-values for responses lacking individual residual records were interpreted subject to the corresponding model assumptions; unreported post-hoc comparisons were not introduced.

Apparent *MDR* was calculated from the complete-track interferometric volume V and the nominal scan duration $t = L/v$, with $L = 6.0$ mm and v expressed in mm/min. The resulting metric represents volume-derived, time-normalized productivity rather than direct weighing or measured Faradaic current efficiency. For the geometrical comparison, Pearson correlation between condition-mean *MDR* and condition-mean H_{max} was calculated across 25 parameter combinations; the correlation was not interpreted causally.

For application-oriented operating-condition selection, each of the 25 experimental mean vectors [*MDR, Ra, Wa*] was evaluated using Pareto dominance. The three objectives were to maximize *MDR* and minimize *Ra* and *Wa*. A condition was classified as dominated if another experimental combination performed at least as well for all objectives and strictly better for at least one. The remaining combinations were designated non-dominated. This classification used the unrounded means; *sd*, *CV*, and H_{max} were retained for interpretation but were not included as dominance objectives. Therefore, the results describe a mean-based experimental Pareto set and do not imply a statistically certain ordering or continuous Pareto frontier.

As an exploratory interpolation analysis, separate full quadratic polynomial models were fitted by ordinary least squares to the 25 condition means of *MDR*, *Ra*, and *Wa*, with predictors i, v, i^2, v^2, and iv plus an intercept. R^2, adjusted R^2, overall *F-test* significance, and an approximately leave-one-condition-out cross-validated predictive R^2 were calculated for each response. Lack of fit was evaluated against pure error reconstructed from the five-replicate *sd's* (19 and 100 degrees of freedom for lack of fit and pure error, respectively); model predictions were restricted to the tested i–v domain. Since all evaluated quadratic models showed significant lack of fit, continuous model-derived optima were not used to recommend untested operating conditions.

3. RESULTS AND DISCUSSION

3.1. Material Deposition Rate

Figure 2 summarizes the combined effects of applied current and nozzle scanning speed on the apparent material deposition rate (*MDR*) of single-pass copper tracks

produced by jet electrodeposition. Figure 2(a) presents the condition-mean *MDR* and corresponding standard deviations, whereas Fig. 2(b) shows the coefficients of variation (*CV*) obtained from five replicates per experimental combination. Because *MDR* was calculated from interferometrically determined deposit volume and nominal deposition time, the resulting values represent geometrically inferred manufacturing productivity rather than a direct measurement of Faradaic current efficiency.

a)

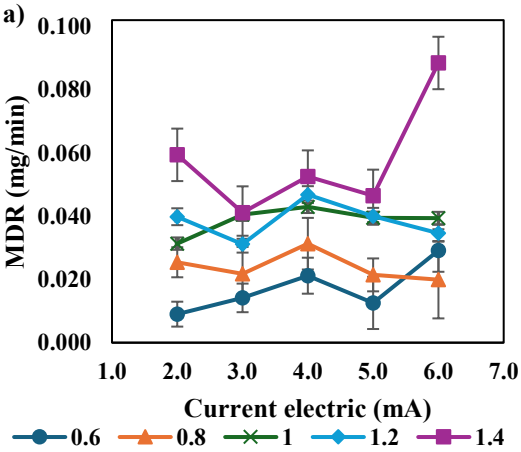

b)

Current electric (mA)	Scan speed (mm/min)				
	0.6	0.8	1	1.2	1.4
2.0	43.70%	18.68%	74.91%	65.96%	22.99%
3.0	31.94%	39.04%	94.69%	60.03%	33.22%
4.0	26.86%	26.07%	31.90%	26.64%	18.31%
5.0	65.65%	24.28%	29.16%	12.72%	5.89%
6.0	23.08%	61.44%	26.80%	13.49%	54.12%

Figure 2. Effect of applied current and nozzle scanning speed on the apparent *MDR* of copper tracks produced by jet electrodeposition: (a) condition-mean MDR ± sample standard deviation (five replicate trials per combination); (b) coefficient-of-variation (CV) heatmap for the 5 × 5 experimental matrix (125 measurements in total).

Nozzle scanning speed exerted a pronounced influence on apparent *MDR*. Averaged across the five current levels, *MDR* increased from 0.017 mg/min at 0.6 mm/min to 0.024 mg/min at 0.8 mm/min, reaching 0.039 mg/min at 1.0 mm/min. A comparable value was observed at 1.2 mm/min (0.039 mg/min), followed by a further increase to 0.058 mg/min at 1.4 mm/min. The overall difference between the lowest and highest scanning speeds corresponded to an increase of 234.5 %. Nevertheless, this trend was not reproduced uniformly at each applied current, indicating that the combined electrochemical and kinematic conditions must be considered rather than scanning speed

The response to applied current was also condition-dependent. At 0.6 mm/min, increasing current from 2 to 6 mA increased apparent *MDR* from 0.009 to 0.029 mg/min. At 0.8 mm/min, however, the corresponding change produced a 21.7 % decrease, with the highest mean at this speed obtained at 4 mA (0.031 mg/min). At 1.4 mm/min, *MDR* increased from 0.059 mg/min at 2 mA to 0.088 mg/min at 6 mA. These contrasting tendencies indicate that a higher imposed current does not necessarily result in a proportionally higher apparent deposition rate across the investigated process window.

The physical interpretation of these results requires distinguishing electrochemical charge delivery from the time normalization embedded in the *MDR* definition. For a fixed track length of 6.0 mm, the nominal processing time is given by $t = L/v$. Increasing scanning speed from 0.6 to 1.4 mm/min therefore decreases deposition time from 10.0 to approximately 4.29 min, a reduction of 57.1 %. Over the same interval, the marginal mean volume-derived mass per track increases from approximately 0.172 to 0.247 mg, corresponding to 43.4 %. Thus, the pronounced increase in apparent *MDR* results from both the shorter processing time and the variation in estimated deposit volume, with the former exerting a particularly strong influence on the rate metric.

Under ideal galvanostatic copper deposition, the Faradaic mass deposition rate is proportional to the imposed current and independent of nozzle translation speed when current efficiency is constant. Conversely, the theoretical amount of copper deposited during a complete track decrease as the processing time becomes shorter. Therefore, the experimentally observed dependence of apparent *MDR* on scanning speed cannot be explained by Faraday's law alone. It may involve changes in the spatial utilization of the imposed current, local electrolyte transport and electrochemical reaction conditions, together with the uncertainties inherent in topographic volume estimation. Since the present study did not independently measure deposited mass, current efficiency, or spatial current-density distributions, these contributions cannot be separated quantitatively.

The localized nature of jet electrodeposition provides a physical basis for such complex behavior. The impinging electrolyte jet establishes a nonuniform electrochemical reaction region, in which current density and ionic mass transfer depend on jet geometry, interelectrode separation, and the distribution of electrolyte flow. Rajput et al. [5] demonstrated through mathematical modeling and experimental validation that the electrical potential distribution within a selective electrodeposition jet governs the predicted deposition rate and deposit height. Kim et al. [16] further reported that imposed current and nozzle-fluid conditions affect copper growth and shape development, while the effect of jetting pressure on growth rate approached saturation above 15 kPa. More recently, Dadi et al. [17] investigated copper microjet deposition through numerical analysis of potential, current-density distribution, and deposition height under changing process conditions. Together, these studies demonstrate that the relationship between electrical input and resulting deposit geometry depends on spatially distributed electrochemical phenomena rather than exclusively on the nominal imposed current.

An additional consideration is the distinction between electrolyte flow rate and nozzle scanning speed. In the present experiments, the nominal electrolyte flow rate was maintained at 2.50 mL/s. Increasing nozzle translation speed consequently did not imply an increase in the volumetric electrolyte supply per unit time. Instead, it changed the duration for which a given substrate region remained exposed to the moving jet and the spatial distribution of electrolyte delivery along the track. Accordingly, improved local ionic replenishment, reduced concentration polarization, or suppression of competing reactions are physically plausible explanations for some observed trends, but they cannot be established directly from the *MDR* measurements.

The repeatability analysis reveals another limitation of selecting operating conditions solely from mean productivity. The lowest *MDR* coefficient of variation was 5.89 % at 5 mA and 1.4 mm/min, corresponding to a mean *MDR* of 0.046 mg/min. In contrast, the condition associated with maximum mean *MDR* (6 mA; 1.4 mm/min; 0.088 mg/min) presented a *CV* of 54.12 %. Thus, an approximately 90.5 % increase in mean apparent productivity at the same scanning speed was accompanied by substantially greater between-track dispersion. The highest *CV* within the experimental matrix was 94.69 %, observed at 3 mA and 1.0 mm/min. Such variability may reflect the combined influence of electrochemical interface evolution, substrate conditions, electrolyte-flow fluctuations, electrical contact, and the sensitivity of the geometrical volume measurement. However, their individual contributions were not measured, preventing identification of a dominant source of experimental scatter.

Two-way ANOVA identified nozzle scanning speed as the predominant factor affecting *MDR* ($F(4,100) = 21.81$, $p < 0.001$; *partial* $\eta^2 = 0.466$). The conventional tests did not identify statistically significant main effects of current ($p = 0.0505$) or current–speed interaction ($p = 0.0965$) at $\alpha = 0.05$. Nevertheless, the residual distribution departed from normality (Shapiro–Wilk, $p = 5.14 \times 10^{-10}$), and heteroscedasticity-consistent HC_3 inference indicated a significant interaction ($p = 0.0108$). Consequently, the influence of scanning speed is comparatively robust, whereas the statistical evidence for interaction depends on the inference procedure. This result reinforces the need to evaluate process variability and model assumptions when interpreting apparent productivity.

Overall, the *MDR* results demonstrate that the highest geometrically inferred production rate is not necessarily associated with the most repeatable operating condition. Moreover, the relationship between current, scanning speed, and apparent deposited mass cannot be reduced to a simple proportional response. The practical implication is that

manufacturing productivity must be interpreted alongside the spatial distribution of deposited material, which is examined through the geometrical characteristics presented in Section 3.2.

3.2. Geometrical characteristics

Figure 3 presents the influence of applied current and nozzle scanning speed on the maximum track height (H_{max}) of single-pass copper tracks produced by jet electrodeposition. Figure 3(a) shows the experimental means and standard deviations, while Fig. 3(b) compares condition-mean H_{max} with apparent *MDR*. Unlike *MDR*, which represents the time-normalized volume of the entire deposited track, H_{max} describes the maximum local vertical extent of the deposit. Consequently, the two quantities characterize different aspects of the manufacturing process and need not exhibit equivalent responses to the operating parameters.

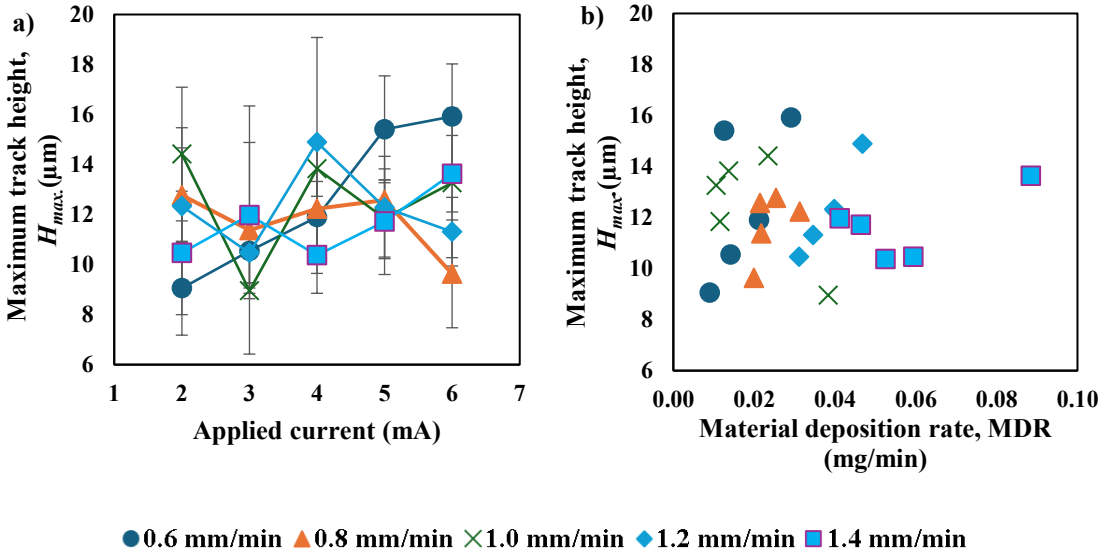

Figure 3. Geometrical response of copper tracks fabricated by jet electrodeposition: (a) mean maximum track height (H_{max}) versus applied current at five nozzle scanning speeds; error bars indicate ±1 sample standard deviation (n = 5 per condition); (b) relationship between condition-mean apparent material deposition rate (MDR) and condition-mean maximum track height (25 conditions). Marker shapes and colors identify scanning speeds.

Mean H_{max} ranged from 8.955 µm at 3 mA and 1.0 mm/min to 15.923 µm at 6 mA and 0.6 mm/min, corresponding to a difference of 77.8 % between the extreme condition means. At the lowest scanning speed, increasing current from 2 to 6 mA increased H_{max} from 9.056 to 15.923 µm (+ 75.8 %). Conversely, at 0.8 mm/min, the same current variation reduced H_{max} from 12.778 to 9.630 µm (− 24.6 %). Reductions of 8.0 % and

8.3 % were also observed at 1.0 and 1.2 mm/min, respectively, whereas at 1.4 mm/min increasing current produced a 30.2 % increase in maximum height. Therefore, the current-induced geometrical response changed substantially with nozzle scanning speed.

When averaged across the five current levels, the influence of scanning speed on H_{max} was comparatively modest. Marginal mean height decreased from 12.569 μm at 0.6 mm/min to 11.633 μm at 1.4 mm/min (− 7.4 %), with non-monotonic values at intermediate speeds. In contrast to the pronounced speed dependence observed for apparent *MDR*, these results indicate that higher time-normalized productivity does not translate directly into greater maximum vertical growth. Importantly, this comparison also suggests that the distribution of deposited material along and across the track must be considered when interpreting manufacturing performance.

The observed behavior can be examined by considering the nominal electrical charge delivered per unit scanning length. For constant imposed current and nozzle speed, this quantity is proportional to i/v. At 6 mA, increasing the scanning speed from 0.6 to 1.4 mm/min decreases the nominal charge supplied per unit length from approximately 0.600 to 0.257 C/mm. In a simplified deposition process with constant current efficiency and an unchanged spatial current-density distribution, the longer local exposure associated with lower scanning speed would favor greater material accumulation in the region traversed by the jet. This scaling is consistent with the highest mean H_{max} being observed at 6 mA and 0.6 mm/min. Nevertheless, it does not establish a universal inverse relationship between scanning speed and maximum height because the current distribution, deposit geometry, and local electrodeposition conditions evolve during processing.

A further consideration is the inherently nonuniform spatial distribution of electrochemical activity beneath an impinging electrolyte jet. The local reduction rate is expected to depend on the distribution of current density, which is affected by electrolyte conductivity, jet geometry, ionic transport, and the electrical boundary conditions at the growing cathodic surface. Preferential deposition near regions of greater local current density may produce locally elevated features without a proportional increase in the volume of the entire track. This interpretation is consistent with the localized-growth patterns discussed in the original experimental investigation [13], although the present measurements do not directly resolve the spatial current-density field or individual growth fronts.

The deposited feature may also modify the electrochemical conditions governing its subsequent growth. Although the initial interelectrode gap was 0.50 mm, the growing copper structure changes the local electrode–electrolyte geometry. Regions of greater height may experience a modified ionic conduction path and altered local current-density distribution. Under galvanostatic control, such changes can affect the cell voltage and current redistribution without requiring variations in the imposed total current. However, maximum measured heights were approximately 9–16 μm, representing only a small fraction of the nominal 500 μm initial gap. Therefore, the contribution of geometrical feedback to the measured height variations cannot be determined without direct measurements of local electrode separation or electrochemical potential evolution.

Previous investigations support the relevance of spatially distributed deposition and nozzle motion to copper-feature geometry. Singh et al. [18] studied electrochemical printing of copper on nickel substrates and reported average deposited-profile heights ranging from 2.56 to 30.46 μm, together with widths from 195.8 to 2401.4 μm, depending on processing conditions. These substantial variations demonstrate that deposited height and lateral dimensions can respond differently to nozzle geometry, scanning speed, and exposure time. Babchuk et al. [19] reported that changing nozzle movement conditions increased the deposited area by nearly 40% in one comparison and produced local thicknesses at trajectory corners up to 2.5 times those in straight sections. Although their deposition geometry and motion strategy differ from the present single-pass tracks, these observations provide direct experimental evidence that nozzle kinematics can redistribute deposited material spatially rather than merely changing its total amount.

Complementary predictive studies provide a mechanistic framework for interpreting this behavior. Kamaraj and Sundaram [12] developed a model incorporating electrical conditions, ion transport, electrode kinetics, and horizontal scanning speed to predict deposition rate and layer height. Their experiments involved deposition rates of approximately 1–3 μm/s and scanning speeds of 0.1–2 mm/s using a 250 μm tool, illustrating an operating regime different from that investigated here. Rajput et al. [5] further demonstrated that potential and electric-field distributions within the electrolyte jet affect predicted deposition height. More recently, Dadi et al. [17] used a two-dimensional numerical model to investigate the evolution of deposition height and current-density distributions during microjet deposition of copper strips. Together, these studies indicate that accurate geometrical prediction may require explicit representation

of evolving deposition boundaries and coupled electrochemical transport rather than a simple relationship between imposed current and final maximum height.

The experimental contrast between productivity and vertical growth is further illustrated in Fig. 3(b). Across the 25 condition means, Pearson correlation between MDR and H_{max} was weak and not statistically significant ($r = 0.122$; $R^2 = 0.015$; $p = 0.561$). At 6 mA and 1.4 mm/min, the highest mean *MDR* (0.088 mg/min) corresponded to $H_{max} = 13.634$ μm. At the same current but a lower speed of 0.6 mm/min, mean *MDR* was approximately 0.0291 mg/min, whereas H_{max} increased to 15.923 μm. Similarly, 5 mA and 0.6 mm/min produced $H_{max} = 15.410$ μm despite a comparatively low *MDR* of approximately 0.013 mg/min. These examples illustrate that greater apparent productivity may coexist with lower peak height, consistent with possible differences in the longitudinal and transverse distribution of deposited material.

Nevertheless, the available measurements do not establish whether such differences result predominantly from lateral spreading, changes in local thickness distribution, isolated height maxima, or other geometrical effects. In particular, H_{max} does not represent mean thickness, and the global *MDR*–H_{max} correlation combines multiple processing conditions. Accordingly, a weak correlation should not be interpreted as evidence that the underlying electrochemical growth processes are independent.

Two-way ANOVA reinforces the condition-dependent nature of vertical growth. Applied current exhibited a significant main effect on H_{max} ($F(4,100) = 3.80$, $p = 0.0064$; *partial* $\eta^2 = 0.132$), whereas the scanning-speed main effect was not significant ($F(4,100) = 0.84$, $p = 0.5005$). More importantly, the current–speed interaction was significant ($F(16,100) = 3.65$, $p = 3.31 \times 10^{-5}$; *partial* $\eta^2 = 0.368$). This comparatively large interaction effect indicates that the response to applied current depends strongly on the nozzle scanning condition. Because the ANOVA was reconstructed from condition means and standard deviations, the statistical interpretation remains subject to assumptions that could not be completely assessed from individual height residuals.

From a manufacturing perspective, these findings demonstrate that maximizing time-normalized material deposition does not ensure maximum vertical feature development or geometrical uniformity. Current and nozzle scanning speed affect the balance between local exposure, electrochemical growth, and spatial material distribution. Thus, H_{max} provides complementary information to *MDR*, and both should be considered when selecting operating conditions for geometrically controlled copper tracks. Further quantitative assessment of track width, transverse cross-sections, and spatial height

distributions would be needed to establish the relative contributions of vertical accumulation and lateral spreading.

3.3. Surface integrity

Figure 4 illustrates the combined influence of applied current and nozzle scanning speed on the surface texture of single-pass copper tracks produced by jet electrodeposition. Figure 4(a) presents the arithmetic mean height of the roughness profile (*Ra*), whereas Fig. 4(b) shows the arithmetic mean height of the waviness profile (*Wa*). Both parameters are reported as means and standard deviations from five replicates per experimental condition. Their combined assessment provides complementary information on surface irregularities associated with different spatial wavelength ranges and enables a more comprehensive evaluation of the relationships between processing conditions and the resulting deposit topography.

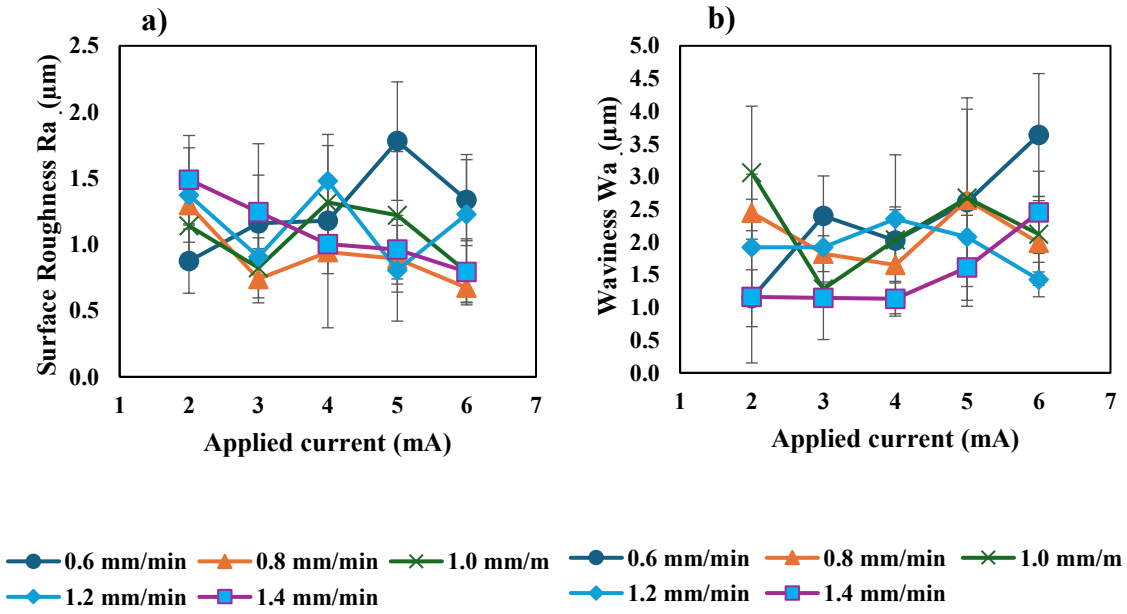

Figure. 4. Combined effects of applied current and nozzle scanning speed on the surface texture of copper tracks manufactured by jet electrodeposition: (a) arithmetic mean height of the roughness profile (*Ra*); (b) arithmetic mean height of the waviness profile (*Wa*). Values represent means ± standard deviations of five replicates per condition. Different marker colors and shapes identify the nozzle scanning speeds.

The *Ra* values ranged from 0.673 ± 0.108 µm at 6 mA and 0.8 mm/min to 1.780 ± 0.447 µm at 5 mA and 0.6 mm/min, corresponding to a 62.2 % reduction from

the highest to the lowest condition mean. As shown in Fig. 4(a), the influence of applied current depended strongly on nozzle scanning speed. At 0.6 mm/min, increasing current from 2 to 6 mA increased *Ra* from 0.874 to 1.335 μm (+ 52.8 %), with the highest value occurring at 5 mA. Conversely, the same current variation reduced *Ra* from 1.297 to 0.673 μm (− 48.1 %) at 0.8 mm/min and from 1.489 to 0.793 μm (− 46.7 %) at 1.4 mm/min. These contrasting responses indicate that increasing current does not systematically promote smoother or rougher deposits; its influence depends on the combined electrochemical and scanning conditions.

When averaged across the five current levels, the lowest marginal mean *Ra* was obtained at 0.8 mm/min (0.908 μm), representing a 28.2 % reduction relative to 0.6 mm/min (1.266 μm). Increasing scanning speed to 1.4 mm/min resulted in a marginal mean *Ra* of 1.098 μm, approximately 20.9 % higher than at 0.8 mm/min. This non-monotonic response suggests that intermediate scanning speeds may provide favorable conditions for reducing roughness amplitude.

A distinct response was observed for *Wa*, which value varied from 1.133 ± 0.266 μm at 4 mA and 1.4 mm/min to 3.637 ± 0.939 μm at 6 mA and 0.6 mm/min, corresponding to a 68.8 % reduction from the highest to the lowest condition mean. At 0.6 mm/min, increasing current from 2 to 6 mA increased *Wa* from 1.141 to 3.637 μm (+ 218.7 %). In contrast, the same current variation at 0.8 mm/min reduced *Wa* from 2.450 to 1.987 μm (− 18.9 %). At 1.4 mm/min, *Wa* exhibited a non-monotonic response, reaching its minimum at 4 mA before increasing to 2.455 μm at 6 mA. Thus, the electrical and kinematic parameters affected longer-wavelength surface irregularities through a strongly condition-dependent response.

The marginal mean *Wa* decreased from 2.362 μm at 0.6 mm/min to 1.502 μm at 1.4 mm/min, corresponding to a relative reduction of 36.4 %. Over the same scanning-speed interval, marginal mean *Ra* decreased by 13.2 %. Although these relative changes indicate different responses of the two profile-texture descriptors to the investigated processing conditions, they should not be interpreted as directly comparable measures of physical sensitivity, since *Ra* and *Wa* are calculated from distinct spatial-wavelength components. Nevertheless, the results demonstrate that the assessment of roughness alone may overlook longer-wavelength surface irregularities relevant to the geometrical consistency of jet-electrodeposited copper tracks.

Two-way analysis of variance confirmed statistically significant effects of nozzle scanning speed ($F(4, 100) = 3.87$, $p = 0.0058$), applied current ($F(4, 100) = 3.37$, $p =$

0.0124), and their interaction ($F(16, 100) = 3.47$, $p < 0.001$) on *Ra*. The corresponding partial eta-squared values were 0.134, 0.119, and 0.357, respectively. Significant effects were also identified for *Wa*, including scanning speed ($F(4, 100) = 5.29$, $p < 0.001$), current ($F(4, 100) = 3.75$, $p = 0.0069$), and the current–speed interaction ($F(16, 100) = 3.57$, $p < 0.001$), with partial eta-squared values of 0.175, 0.130, and 0.363, respectively. The comparatively large interaction effect sizes demonstrate that the responses of both texture parameters to applied current depend on the selected scanning speed. Therefore, the observed trends should not be reduced to isolated main effects or interpreted as monotonic relationships across the entire experimental domain. These conventional factorial ANOVA results were reconstructed from the validated condition means, sample standard deviations, and five replicates per condition; direct residual diagnostics remain necessary for a complete assessment of the underlying statistical assumptions.

The within-condition dispersion also revealed differences in process repeatability. For *Ra*, the condition of 3 mA and 0.8 mm/min exhibited a coefficient of variation (*CV*) of 4.23 %, whereas the condition with the lowest mean *Ra* (6 mA and 0.8 mm/min) presented a CV of 16.07 %. For *Wa*, the condition of 5 mA and 0.8 mm/min exhibited a *CV* of 3.10 %, despite a mean *Wa* of 2.646 μm. Conversely, the condition associated with the lowest mean *Wa* (4 mA and 1.4 mm/min) presented a *CV* of approximately 23.46 %. These findings demonstrate that minimizing the mean surface-texture amplitude does not necessarily minimize trial-to-trial variability. Consequently, both response magnitude and repeatability should be considered when identifying suitable processing conditions.

From an electrochemical perspective, the non-monotonic roughness response may result from competing effects of interfacial charge-transfer kinetics, Cu^{2+} transport, nucleation, and preferential deposit growth. Under galvanostatic conditions, increasing the applied current changes the electrochemical demand for charge transfer and may modify cathodic polarization and the spatial distribution of local growth sites. Depending on the prevailing transport and interfacial conditions, enhanced nucleation and subsequent coalescence may reduce surface irregularities. Conversely, nonuniform current-density distribution, local concentration gradients, and preferential growth at protrusions may increase roughness amplitude. Since nozzle scanning speed determines the local duration of electrolyte exposure during translation, variations in current and speed may modify the balance between electrochemical reaction rates, ion availability, and spatial deposition uniformity. The statistically significant interaction identified for Ra

is consistent with this coupled behavior, although the contribution of each individual mechanism was not independently quantified.

The waviness response requires an additional interpretation because it describes longer-wavelength deviations of the longitudinal surface profile. Unlike roughness, which primarily captures shorter-wavelength irregularities, waviness may reflect the spatial evolution of deposition along the scanning trajectory. The original doctoral investigation [13] reported wave-like topographical features and successive localized growth regions, interpreted as the development and displacement of preferential deposition fronts during nozzle translation. These observations suggest that waviness may be associated not only with electro crystallization but also with the kinematic characteristics of the deposition system and their interaction with the evolving electrochemical interface. However, *Wa* is an amplitude-based descriptor and does not independently establish spatial periodicity or identify the physical origin of the observed profile variations.

One possible mechanism involves changes in the effective interelectrode gap (IEG) during track formation. Although the nominal initial IEG was fixed at 0.50 mm, the growth of the copper deposit progressively modifies the local electrode–electrolyte geometry. Additional variations could arise from substrate flatness, nozzle–substrate positioning errors, or dynamic relative displacement during scanning. These effects may alter the effective ionic conduction path and the associated ohmic potential drop. Under the galvanostatic operating mode employed here, the total current is controlled by the power supply, which adjusts the cell potential within its operating limits. Consequently, changes in the effective gap should not be interpreted as direct fluctuations in imposed total current. Instead, they may modify the required cell voltage, local current-density distribution, and interfacial polarization, potentially redistributing the rate of copper reduction across the active deposition region.

This interaction introduces a possible feedback mechanism between deposited topography and local electrochemical conditions. Preferential growth at a particular location may alter the local conduction path and electric-field distribution, which could further influence subsequent deposition. If such changes occur repeatedly or unevenly along the scanning trajectory, they may contribute to longer-wavelength surface irregularities. Nevertheless, the magnitude of this contribution cannot be established from *Wa* measurements alone. The measured track heights represent only a relatively small fraction of the nominal 500 μm gap, and the actual ohmic response also depends on jet

geometry, electrolyte conductivity, and the distribution of current paths. Therefore, dynamic IEG variations and their potential influence on waviness remain physically plausible, but experimentally unverified, mechanisms in the present study.

Previous investigations provide support for this electrochemical interpretation. Kim et al. [16] demonstrated that, under constant-current jet-assisted copper deposition, changes in the distance between the working electrode and nozzle altered the voltage response while the imposed current remained approximately constant. Bisterov et al. [20], working with electrochemical jet machining rather than deposition, demonstrated that the electrical resistance of an impinging electrolyte jet depends on nozzle-to-surface distance and can be used for on-machine topographical measurement. More recently, Xiang et al. [7] developed a closed-loop Jet ECD system using image recognition and voltage feedback to coordinate deposition growth and nozzle positioning. Although these investigations involve different process configurations, they demonstrate the physical relevance of coupling between electrode separation, electrical response, and nozzle motion. In the present experiments, however, no direct measurement of dynamic IEG, positioning oscillations, or spatially resolved current density was performed, preventing identification of their individual contributions to the measured *Wa* values.

A related factor is the spatial distribution of electrolyte flow and its effect on ionic mass transport. Under continuous jet delivery, the local hydrodynamic field governs the renewal of electroactive species and may influence concentration gradients near the growing copper surface. Changes in the active deposition region during nozzle translation can therefore modify the relationship between mass transport and electrochemical reaction rate. The original experimental observations of lateral spreading and heterogeneous growth are compatible with this interpretation. Nevertheless, identifying a specific hydrodynamic instability or mechanically induced oscillation would require synchronized flow, motion, or electrochemical measurements beyond the scope of the present investigation.

The surface-texture results were compared with previous studies involving localized electrochemical additive manufacturing of copper, as summarized in Table 2. Since the studies employ different substrates, nozzle configurations, electrolytes, deposition strategies, and surface-characterization techniques, the reported values are intended to provide technological context and identify methodological gaps rather than establish a direct ranking of surface quality.

Table 2. Comparison of reported copper surface-texture characteristics in electrochemical additive manufacturing.*

Study	Process and characterization	Reported surface-texture result	Relevance and limitations
Present study	Single-pass copper Jet ECD on Cu; longitudinal profile characterization	Minimum Ra = 0.673 ± 0.108 µm; minimum Wa = 1.133 ± 0.266 µm	Replicated 5 × 5 factorial investigation of roughness, waviness, and current–speed interactions
Arshad et al. [6]	Free-flow jet micro-ECAM of Cu on stainless steel	Minimum reported surface roughness = 0.38 ± 0.02 µm	Related localized deposition process; the accessible publisher abstract does not specify whether the reported parameter is Ra or Sa
Li et al. [10]	Jet electrodeposition of Cu on Ni using different nozzle geometries; areal topography	Sa decreased from 5.40 to 2.76 µm	Demonstrates the influence of electrolyte-flow distribution on surface morphology and deposition localization
Gu et al. [9]	High-speed circulating electrolyte-jet printing of Cu microelectrodes; AFM	Minimum Ra = 1.1 nm	Demonstrates the influence of nucleation and local current-density conditions at a different measurement scale
Dong et al. [11]	Jet ECD of copper mesostructures; optimized electrolyte additives, processing conditions, and substrate modification	Sa ≈ 65 nm for copper columns; average Sa ≈ 0.20 µm for planar structures	llustrates surface-quality optimization by electrolyte chemistry and processing strategy
Xiang et al. [7]	Closed-loop Jet ECD of copper microstructures using image recognition and voltage feedback	Ra = 18.54 nm	Demonstrates the technological relevance of coordinating electrochemical growth and nozzle positioning

* Notes: Ra and Wa are profile parameters, whereas Sa is an areal parameter. Their values are not directly interchangeable. The values also refer to different measurement scales, evaluation lengths or areas, filtering conditions, deposition strategies, and substrate materials. The surface-roughness parameter designation in Arshad et al. [6] is not specified in the accessible publisher abstract.

As shown in Table 2, Arshad et al. [6] demonstrated localized copper deposition using a free-flow jet micro-electrochemical additive manufacturing system and reported a minimum surface roughness of 0.38 ± 0.02 µm. Their findings establish the importance of surface quality in evaluating the performance of localized electrochemical manufacturing. However, the differences in substrate material, operating conditions, and available roughness definitions limit direct numerical comparisons with the present measurements.

The technological relevance of waviness in jet electrodeposition has also been recognized in earlier investigations. Rajput et al. [21] reported waviness amplitudes on the order of 10–50 µm during ultrasonic-assisted jet electrodeposition, highlighting the persistence of geometrical irregularities even when improvements in dimensional

accuracy were achieved. Although these measurements cannot be directly compared with the filtered *Wa* values obtained in the present investigation because of differences in deposition conditions, feature geometry, and parameter definitions, they demonstrate that longer-wavelength irregularities are an established concern in localized electrochemical manufacturing. The contribution of the present study lies in quantitatively evaluating longitudinal *Wa* alongside *Ra*, apparent *MDR*, and process repeatability within a replicated current–speed factorial design.

Li et al. [10] investigated the effects of nozzle geometry and flow-field distribution on copper deposits produced by jet electrodeposition. By modifying the aspect ratio of rectangular nozzles, the authors reported a reduction in areal roughness from *Sa* = 5.40 to 2.76 μm, accompanied by fewer nodular deposits and improved deposition localization. These observations provide experimental support for the importance of electrolyte-flow uniformity in controlling deposit morphology. In the present investigation, nozzle geometry and nominal flow rate were maintained constant; therefore, the observed texture variations are interpreted primarily in relation to applied current and scanning speed, although local hydrodynamic conditions may still vary during deposition.

Gu et al. [9] demonstrated the production of ultrasmooth copper microelectrodes using a high-speed circulating electrolyte-jet system, reporting a minimum AFM-measured *Ra* of 1.1 nm. Their results highlighted the influence of cathodic current-density fluctuations and nucleation behavior on copper surface morphology. Importantly, these findings indicate that surface roughness depends on the spatial organization of deposited material rather than exclusively on the magnitude of the imposed electrical parameters. Nevertheless, differences in deposition strategy and measurement scale preclude direct comparison with the micrometric longitudinal roughness profiles investigated here.

Recent developments further reinforce the technological importance of electrochemical and process control. Dong et al. [11] investigated electrolyte additives, processing parameters, and cathode surface modification to improve the surface quality and efficiency of jet-electrodeposited copper meso structures. Their optimized conditions produced copper columns with areal roughness values of approximately 65 nm and planar structures with average *Sa* values near 0.20 μm. These results highlight the effectiveness of electrolyte chemistry and surface preparation as additional control variables, although they do not establish the behavior of longitudinal waviness under the current–speed combinations investigated here.

Xiang et al. [7] addressed a complementary limitation of Jet ECD by implementing a closed-loop strategy based on image recognition and voltage feedback. Their system coordinated nozzle movement with the evolving copper deposit geometry, demonstrating that electrical feedback can improve the control of complex three-dimensional structures. This contribution is particularly relevant to the present discussion of waviness because it confirms the importance of coordinating spatial motion with electrochemical growth. However, the authors did not establish a quantitative relationship between *Wa* and dynamic variations in IEG or nozzle positioning. Accordingly, their results support the proposed coupling mechanism without directly validating it for the present copper tracks.

The comparison in Table 2 reveals a relevant distinction in the existing literature. The studies considered predominantly emphasize roughness amplitude, surface morphology, deposition localization, and dimensional accuracy. In contrast, quantitative waviness characterization, particularly when combined with replicated factorial analysis of scanning speed and applied current, is less prominently documented. This represents a meaningful methodological gap because longer-wavelength surface irregularities may contain information on spatial deposition uniformity and potentially on the interaction between nozzle kinematics, effective electrode separation, and electrochemical growth that cannot be inferred from *Ra* alone.

The present investigation contributes to addressing this gap by demonstrating statistically significant current–speed interactions for both *Ra* and *Wa* under the same experimental matrix, while identifying distinct operating conditions associated with their minimum values. The findings support the use of waviness as a complementary response variable for evaluating the spatial consistency of jet-electrodeposited tracks. Nevertheless, attributing the measured waviness to specific mechanical, electrical, or hydrodynamic disturbances requires additional evidence, including dynamic nozzle-position measurements, galvanostatic potential monitoring, or spatial-frequency analysis of the original longitudinal profiles.

Therefore, the principal contribution of the surface-integrity assessment is not the achievement of an unprecedented minimum roughness value, but the systematic characterization of distinct surface-texture responses under controlled and replicated processing conditions. By linking the observed roughness and waviness behavior to physically plausible electrochemical and kinematic mechanisms, the results provide a basis for understanding the coupled influences of applied current and nozzle motion. Combined with the *MDR* and maximum track-height analyses presented in Sections 3.1

and 3.2, these findings establish an experimental framework for multi-response optimization of jet electrochemical additive manufacturing, balancing deposition productivity, geometrical growth, surface texture, and process repeatability.

3.4. Application-oriented parameter selection and multi-response trade-off's

The combined results for material deposition rate (*MDR*), surface roughness (*Ra*), and waviness (*Wa*) indicate that the selection of jet electrodeposition parameters is inherently application-dependent. As demonstrated in Sections 3.1–3.3, increasing current or nozzle scanning speed does not produce uniformly favorable changes in all three responses. Accordingly, the present section uses the complete factorial dataset to identify experimentally observed response extrema and non-dominated operating conditions rather than imposing a universal optimum.

Six individual optimization objectives were first considered: maximizing and minimizing *MDR*, *Ra*, and *Wa*. Among the 25 tested conditions, the highest mean *MDR* (0.08845 mg/min) was obtained at 6 mA and 1.4 mm/min, whereas the lowest mean *Ra* (0.6729 μm) occurred at 6 mA and 0.8 mm/min and the lowest mean *Wa* (1.1331 μm) at 4 mA and 1.4 mm/min. The minimum *MDR* (0.00902 mg/min), maximum *Ra* (1.780 μm), and maximum *Wa* (3.637 μm) occurred at 2 mA;0.6 mm/min, 5 mA; 0.6 mm/min, and 6 mA;0.6 mm/min, respectively. These extremes are descriptors of the investigated processing space, not interchangeable indicators of product quality. In particular, a lower deposition rate is not intrinsically preferable, and increased *Ra* or *Wa* does not demonstrate improved adhesion or electrochemical activity without functional testing.

To identify conditions offering competitive compromises, a Pareto dominance analysis was performed on all 25 experimental means using three simultaneous objectives: maximizing *MDR* and minimizing *Ra* and *Wa*. A condition was classified as non-dominated when no other tested combination provided at least equivalent performance in all three responses and a strict improvement in at least one. Ten non-dominated conditions were identified, as summarized in Table 3. Maximum track height (H_{max}), standard deviations, and coefficients of variation were retained as complementary descriptors but were not used to determine Pareto dominance. Therefore, the resulting front represents performance trade-offs among the three selected mean responses, not a comprehensive optimum of geometrical or functional properties.

Table 3. Experimentally non-dominated conditions obtained by maximizing mean *MDR* and minimizing mean *Ra* and *Wa*. Mean ± sample standard deviation (n = 5) and *CV* are reported for the optimization responses; H_{max} is complementary and was not used for Pareto dominance.

i **(mA)**	***v*** **(mm/min)**	***MDR*** **(mg/min)** ***mean ± sd; CV***	***Ra*** **(µm)** ***mean ± sd; CV***	***Wa*** **(µm)** ***mean ± sd; CV***	H_{max} **(µm)** ***mean ± sd***
2	0.6	0.0090 ± 0.0039 CV 43.7%	0.874 ± 0.242 CV 27.7%	1.141 ± 0.435 CV 38.1%	9.056 ± 1.877
3	0.8	0.0218 ± 0.0085 CV 39.0%	0.738 ± 0.031 CV 4.2%	1.822 ± 0.274 CV 15.0%	11.383 ± 4.961
6	0.8	0.0199 ± 0.0122 CV 61.4%	0.673 ± 0.108 CV 16.1%	1.986 ± 0.647 CV 32.6%	9.630 ± 2.156
3	1.0	0.0405 ± 0.0383 CV 94.7%	0.823 ± 0.227 CV 27.5%	1.282 ± 0.074 CV 5.8%	8.955 ± 0.318
6	1.0	0.0394 ± 0.0106 CV 26.8%	0.794 ± 0.234 CV 29.5%	2.119 ± 0.576 CV 27.2%	13.266 ± 2.988
5	1.2	0.0400 ± 0.0051 CV 12.7%	0.806 ± 0.384 CV 47.7%	2.074 ± 0.335 CV 16.1%	12.283 ± 2.046
2	1.4	0.0594 ± 0.0137 CV 23.0%	1.489 ± 0.334 CV 22.4%	1.162 ± 1.011 CV 86.9%	10.468 ± 2.469
4	1.4	0.0525 ± 0.0096 CV 18.3%	1.002 ± 0.222 CV 22.2%	1.133 ± 0.266 CV 23.5%	10.374 ± 1.521
5	1.4	0.0464 ± 0.0027 CV 5.9%	0.960 ± 0.260 CV 27.0%	1.611 ± 0.501 CV 31.1%	11.716 ± 2.111
6	1.4	0.0884 ± 0.0479 CV 54.1%	0.793 ± 0.249 CV 31.4%	2.455 ± 0.627 CV 25.6%	13.634 ± 1.530

Distinct operating strategies emerged within the non-dominated set. The condition of 4 mA and 1.4 mm/min yielded the minimum *Wa* (1.133 ± 0.266 µm), with a mean *MDR* of 0.05252 ± 0.00962 mg/min and *Ra* of 1.0017 ± 0.2222 µm. It's *CV's* for *MDR*, *Ra*, and *W*a were 18.3 %, 22.2 %, and 23.5 %, respectively, indicating an absence of extreme relative dispersion in these three responses. By contrast, 5 mA and 1.4 mm/min exhibited the lowest *MDR* coefficient of variation among all 25 tested combinations (5.89 %), with *MDR* = 0.04642 mg/min. The maximum-productivity condition, 6 mA and 1.4 mm/min, reached a mean *MDR* approximately 90.5 % higher than that at 5 mA and the same speed, but its *MDR* coefficient of variation increased to 54.1 %. These observations distinguish high average throughput from between-track repeatability, without establishing a time-resolved measure of process stability. Because *MDR* is normalized by processing time, scanning-speed-related differences in *MDR* must also be interpreted alongside the actual deposited mass and track geometry, rather than solely as changes in electrochemical growth kinetics.

The selection of process parameters from separate response curves can obscure experimentally available improvements. For example, relative to 4 mA and 1.0 mm/min, the combination of 4 mA and 1.4 mm/min increased mean *MDR* by 22.2 % while reducing *Ra* by 24.0 % and *Wa* by 44.3 %. Thus, the latter condition dominates the former in the

selected three-response space, although the conditions may differ in height, morphology, or other properties not included in the dominance criterion. Figure 5 visualizes this trade-off using *MDR* and *Ra* as axes, *Wa* as a color-coded response, and distinct symbols for dominated and non-dominated conditions.

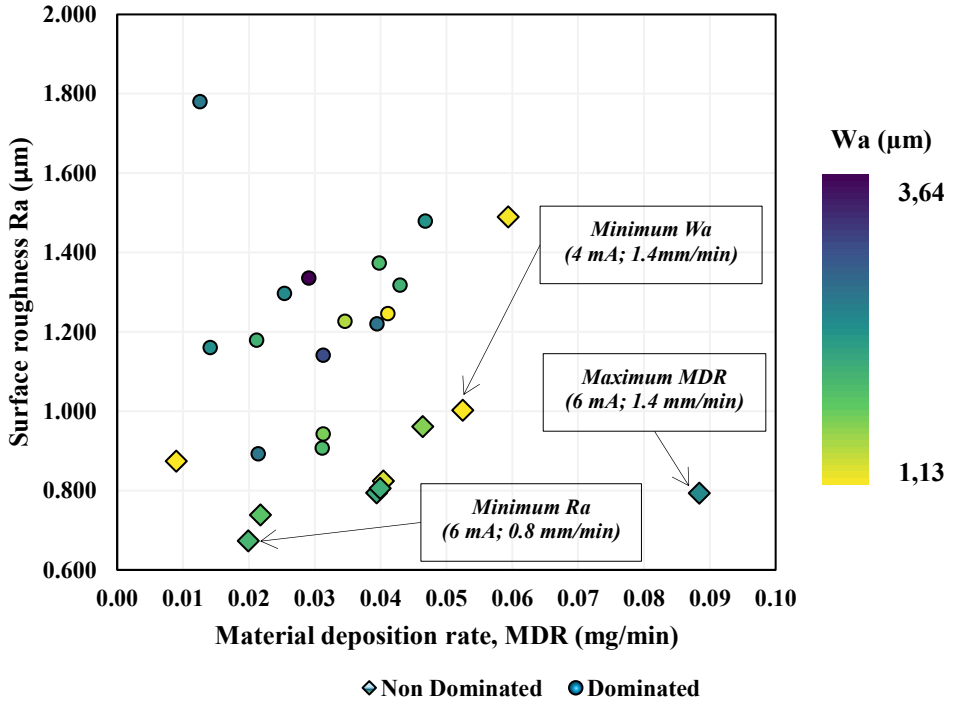

Figure. 5. Experimental Pareto classification of copper tracks produced by jet electrodeposition. Material deposition rate (*MDR*) and arithmetic mean profile roughness (*Ra*) are represented on the horizontal and vertical axes, respectively, while marker color indicates arithmetic mean profile waviness (*Wa*). Diamond markers identify the ten non-dominated conditions, whereas circular markers represent the fifteen dominated conditions. Pareto dominance was determined by maximizing MDR and simultaneously minimizing *Ra* and *Wa*, considering the mean values obtained from five experimental replicates per condition. The operating conditions corresponding to maximum *MDR*, minimum *Ra*, and minimum *Wa* are highlighted.

A second-order polynomial response-surface analysis was also evaluated as a potential basis for interpolation within the experimental domain. The corrected models used current, scanning speed, their squared terms, and their interaction as predictors. The *MDR* model captured the main trend in the condition means ($R^2 = 0.715$; *adjusted* $R^2 = 0.640$; overall $p = 0.00011$), whereas models for *Ra* ($R^2 = 0.272$; *adjusted* $R^2 = 0.081$) and *Wa* ($R^2 = 0.351$; *adjusted* $R^2 = 0.180$) showed limited explanatory performance. Significant lack-of-fit tests were obtained for all three models ($p < 0.05$) and leave-one-condition-out cross-validation gave predictive R^2 values of 0.300, −0.173, and −0.437 for *MDR*, *Ra*, and *Wa*, respectively. Consequently, the quadratic equations were not considered sufficiently reliable to propose untested continuous optima. The Pareto

analysis was therefore restricted to the experimentally investigated parameter combinations.

The limitations identified in the quadratic response-surface models should be interpreted in the context of previous predictive and optimization approaches for jet-based electrochemical additive manufacturing. Table 4 summarizes representative investigations and distinguishes physics-based deposition modeling, empirically supported process optimization, and real-time feedback control.

Table 4. Comparison of modeling, optimization, and process-control approaches reported for jet-based electrochemical additive manufacturing.

Study	Approach	Main process variables	Evaluated or predicted responses	Relevance to the present study
Rajput et al. [5]	Physics-based mathematical modeling and finite-element simulation, experimentally validated	Applied voltage, electrolyte concentration, interelectrode gap	Deposition rate, deposit height, electrical potential distribution	Establishes a mechanistic framework for predicting deposition behavior
Kamaraj and Sundaram [12]	Mathematical modeling incorporating ion transport and electrode kinetics	Electrical parameters, horizontal scanning speed, interelectrode gap	Deposition rate and layer height	Demonstrates the importance of nozzle translation in deposition prediction
Dadi et al. [17]	Two-dimensional numerical simulation and experimental parametric investigation	Applied voltage, feed rate, electrolyte flow rate	Deposited height, potential and current-density distributions	Relates electrochemical transport to spatial deposition characteristics
Xiang et al. [22]	Image-based monitoring and feedback control	Deposition time, nozzle displacement, observed deposition-front position	Growth evolution and geometrical control	Addresses nonlinear deposition behavior through real-time feedback
Dong et al. [11]	Taguchi design and response-surface methodology with experimental validation	Electrolyte additives, composition, current density, surface preparation	Surface precision and deposition efficiency	Demonstrates experimentally supported process optimization with multiple performance considerations
Xiang et al. [7]	Closed-loop control combining image recognition and voltage feedback	Nozzle positioning, voltage response and deposition evolution	Geometrical accuracy and controlled 3D copper growth	Demonstrates coupling between electrochemical response and motion control
Present study	Replicated factorial experiments, quadratic-model assessment and	Applied current (2–6 mA), scanning speed (0.6–1.4 mm/min)	MDR, Ra, Wa; Hmax as supplementary descriptor	Identifies experimentally non-dominated operating conditions and evaluates repeatability without

Study	Approach	Main process variables	Evaluated or predicted responses	Relevance to the present study
	empirical Pareto analysis			relying on inadequately validated interpolated optima

Note: The studies differ in electrical control mode, deposition geometry, materials, response definitions, and measurement units. The table compares methodological approaches and investigates objectives rather than numerical prediction accuracy or absolute deposition performance.

Rajput et al. [5] developed and experimentally validated a mathematical framework capable of predicting deposition rate and height through the distribution of electric potential within the electrolyte jet. Kamaraj and Sundaram [12] subsequently incorporated horizontal scanning speed into a model that considered electrochemical transport and reaction kinetics, while Dadi et al. [17] combined numerical simulation with experimental characterization of copper microjet deposition. These studies demonstrate that accurate prediction of deposition behavior may require explicit consideration of the electrochemical and transport phenomena governing local material growth. However, their models, operating regimes, and response definitions differ from those examined in the present investigation, preventing direct comparison of prediction errors or deposition-rate values.

More recently, Xiang et al. [7, 22] employed image-based monitoring and electrical feedback to address nonlinear deposition behavior and coordinate copper growth with nozzle displacement. Their findings emphasize the importance of considering the evolving deposition geometry rather than assuming a fixed relationship between operating parameters and local growth rate. Dong et al. [11], in turn, demonstrated the applicability of Taguchi experiments and response-surface methodology to improving deposition efficiency and surface precision through optimization of electrolyte chemistry, current density, and surface preparation.

Unlike those studies, the present investigation does not seek to establish a comprehensive mechanistic model or a real-time control strategy. Instead, it uses a replicated factorial dataset to determine which experimentally tested current–speed combinations offer competitive compromises among mass-based productivity, roughness, and waviness. The inadequate predictive performance of the evaluated quadratic models therefore motivates the use of an empirical Pareto classification rather than extrapolation toward unverified operating conditions. This provides a transparent framework for selecting processing parameters while acknowledging the limitations of empirical interpolation and the need for application-specific functional validation.

From an application-oriented viewpoint, the present results suggest alternative experimental operating windows rather than a unique optimum. The 6 mA;1.4 mm/min condition provides the highest mean *MDR* when throughput is prioritized, and its substantial variability can be tolerated. The 4 mA;1.4 mm/min condition favors lower longitudinal waviness with moderate productivity and comparatively balanced coefficients of variation, whereas 5 mA;1.4 mm/min favors repeatability of mass-based throughput. The 6 mA;0.8 mm/min condition is the lowest *Ra* regime but exhibits comparatively high *MDR* variability. These candidates require application-specific geometrical constraints and functional verification before being recommended for production.

Overall, a mean-based Pareto analysis of the replicated factorial dataset offers a transparent, data-grounded procedure for selecting current–speed combinations for copper Jet ECD. The analysis reveals that productivity, roughness, waviness, and repeatability should be treated as distinct manufacturing considerations. It also identifies a clear boundary between experimentally supported trade-offs and interpolated optima requiring improved predictive models or confirmatory experiments. This framework complements the physical and statistical interpretations developed in Sections 3.1–3.3 without introducing unsupported claims of a universally optimal operating condition.

4. CONCLUSIONS

This study investigated how applied current and nozzle scanning speed jointly influence the apparent material deposition rate, maximum track height, and longitudinal roughness and waviness of copper tracks fabricated by galvanostatic Jet ECD. Based on a replicated 5 × 5 factorial dataset (125 trials) and an experimental Pareto analysis, the following conclusions are drawn:

- Time-normalized productivity and deposited mass are not equivalent. The marginal mean apparent *MDR* increased from 0.0172 to 0.0576 mg/min as scanning speed rose from 0.6 to 1.4 mm/min (+ 234.5 %); over the same interval, the estimated deposited mass per track increased by only 43.4 %. The strong speed effect in conventional ANOVA ($F(4,100) = 21.81$, $p < 0.001$) must therefore be interpreted together with the shorter processing time and the uncertainties associated with converting interferometric volume into mass.

- High average *MDR* entails a repeatability trade-off. The largest mean *MDR* was 0.088 mg/min at 6 mA and 1.4 mm/min, but its *CV* was 54.1 %. At 5 mA and the same speed, *MDR* was 0.046 mg/min with a *CV* of only 5.89 %. Thus, a 90.5 % increase in mean productivity was accompanied by substantially greater between-track scatter.
- Peak height cannot be inferred from *MDR* alone. Mean H_{max} ranged from 8.955 to 15.923 μm across conditions and exhibited a significant current–speed interaction ($F(16,100) = 3.65$, $p < 0.001$). Its correlation with mean *MDR* was weak and not statistically significant ($r = 0.122$, $p = 0.561$), indicating that total time-normalized deposit volume and localized vertical growth are distinct manufacturing responses.
- Roughness and waviness require different process selections. The lowest *Ra* (0.673 ± 0.108 μm) occurred at 6 mA and 0.8 mm/min, whereas the lowest *Wa* (1.133 ± 0.266 μm) occurred at 4 mA and 1.4 mm/min. Significant current–speed interactions were detected for both *Ra* and *Wa* ($p < 0.001$). Across the extreme speed levels, marginal *Wa* decreased by 36.4 %, compared with a 13.2 % decrease in *Ra*, supporting joint assessment of distinct profile-texture components rather than the use of Ra as a standalone quality indicator.
- The experimental Pareto set identifies application-dependent compromises, not a universal optimum. Ten of the 25 conditions were non-dominated when maximizing *MDR* and minimizing *Ra* and *Wa*. The 4 mA;1.4 mm/min condition combined minimum mean *Wa* with *MDR* = 0.053 mg/min and *CV's* of 18.3 %, 22.2 %, and 23.5 % for *MDR*, *Ra*, and *Wa*, respectively. Conditions favoring maximum throughput, minimum *Ra*, or minimum *Wa* differ; none can be declared functionally superior without application-specific geometrical and performance constraints.
- Quadratic interpolation did not support reliable continuous optimization. Although the *MDR* model reached $R^2 = 0.715$, significant lack of fit was identified for *MDR*, *Ra*, and *Wa* ($p < 0.05$), and cross-validated *predictive* R^2 values were approximately 0.300, −0.173, and −0.437, respectively. Accordingly, recommendations were restricted to experimentally tested conditions. Future investigations should assess profile-filtering and acquisition-sampling sensitivity, dynamic IEG and galvanostatic voltage signals, and independent dimensional or functional validation before extending the proposed process windows.

5. REFERENCES

1. PATEL, S.; LIU, Y.; SIDDIQUE, Z.; GHAMARIAN, I. Metal additive manufacturing: Principles and applications. Journal of Manufacturing Processes, 131, 1179–1201, published online 2024. https://doi.org/10.1016/j.jmapro.2024.09.101.

2. AYALEW, A. A.; HAN, X.; SAKAIRI, M. A critical review of additive material manufacturing through electrochemical deposition techniques. Additive Manufacturing, 77, 103796, 2023. https://doi.org/10.1016/j.addma.2023.103796.

3. HENGSTELER, J.; KANES, K. A.; KHASANOVA, L.; MOMOTENKO, D. Beginner's guide to micro- and nanoscale electrochemical additive manufacturing. Annual Review of Analytical Chemistry, 16, 71–91, 2023. https://doi.org/10.1146/annurev-anchem-091522-122334.

4. AKBAR, Z.; HE, M.; LIU, H.; ZHANG, H. Towards micro/nano-electrochemical additive manufacturing: A critical review. Journal of Materials Processing Technology, 350, 119267, 2026. https://doi.org/10.1016/j.jmatprotec.2026.119267.

5. RAJPUT, M. S.; PANDEY, P. M.; JHA, S. Modelling of high speed selective jet electrodeposition process. Journal of Manufacturing Processes, 17, 98–107, 2015. https://doi.org/10.1016/j.jmapro.2014.07.012.

6. ARSHAD, M. H.; SAXENA, K. K.; SMITH, R.; QIAN, J.; REYNAERTS, D. Localized and mask-less copper deposition with free-flow jet micro-electrochemical additive manufacturing. International Journal of Electrical Machining, 27, 16–21, 2022. https://doi.org/10.2526/ijem.27.16.

7. XIANG, W.; CHEN, B.; REN, W.; LIU, B.; LIN, C.; YANG, Y. An automated closed-loop fabrication of 3D microscale metal structures via image recognition and voltage feedback in Jet ECD. Chemical Engineering Journal, 542, 178087, 2026. https://doi.org/10.1016/j.cej.2026.178087.

8. YE, P.; NIU, Q.; WANG, F. Effect of electrolyte composition and deposition voltage on the deposition rate of copper microcolumns jet electrodeposition. Materials Science and Engineering: B, 298, 116857, 2023. https://www.sciencedirect.com/science/article/pii/S0921510723005998.

9. GU, W.; MARIANOV, A.; JIANG, Y. High-speed electrolyte jet 3D printing of ultrasmooth and robust Cu microelectrodes. Journal of Materials Science, 59, 4605–4619, 2024. https://doi.org/10.1007/s10853-024-09514-7.

10. LI, Z.; PENG, W.; WANG, Y.; FANG, T. Effect of flow field changes on copper deposition layer during jet electrodeposition. Surface Technology, 53(14), 207–215, 2024. https://doi.org/10.16490/j.cnki.issn.1001-3660.2024.14.020.

11. DONG, P.; LIU, Y.; CHEN, L.; LI, W.; TANG, J. Enhancing surface quality and efficiency of copper meso-structures in jet electrodeposition. Surfaces and Interfaces, 81, 108445, 2026. https://doi.org/10.1016/j.surfin.2026.108445.

12. KAMARAJ, A. B.; SUNDARAM, M. A mathematical model of the deposition rate and layer height during electrochemical additive manufacturing. The International Journal of Advanced Manufacturing Technology, 102, 2367–2374, 2019. https://doi.org/10.1007/s00170-019-03292-2.

13. AMARAL, L. B. do. Desenvolvimento e caracterização de sistema de eletrodeposição por jato para manufatura aditiva eletroquímica: investigação experimental dos efeitos de parâmetros de processo na qualidade de depósitos de cobre. Tese (Doutorado em Engenharia Mecânica), Universidade Federal de Uberlândia, Uberlândia, 2025. https://doi.org/10.14393/ufu.te.2026.107.

14. ISO. ISO 21920-2:2021. Geometrical product specifications (GPS)—Surface texture: Profile—Part 2: Terms, definitions and surface texture parameters. International Organization for Standardization, Geneva, 2021. https://www.iso.org/standard/72226.html.

15. ISO. ISO 21920-3:2021. Geometrical product specifications (GPS)—Surface texture: Profile—Part 3: Specification operators. International Organization for Standardization, Geneva, 2021. https://www.iso.org/standard/72228.html.

16. KIM, Y.-K. et al. The characteristics of selective 3D metal additive process using electrochemical deposition and nozzle fluid dynamics. Frontiers in Mechanical Engineering, 6, 9, 2020. https://doi.org/10.3389/fmech.2020.00009.

17. DADI, S. S. O.; PATEL, D.; BAFNA, N.; GARG, G. K. Localised electrochemical additive manufacturing via microjet electrochemical deposition. Journal of The Electrochemical Society, 172(4), 042506, 2025. https://doi.org/10.1149/1945-7111/adcd01.

18. SINGH, M.; MOHANTY, S.; DAS, A. K. Parametric analysis to enhance the printability in metal with electrochemical additive manufacturing. Materials Letters, 322, 132518, 2022. https://doi.org/10.1016/j.matlet.2022.132518.

19. BABCHUK, R. et al. Additive concentration and nozzle moving speed influence on local copper deposition for electrochemical 3D-printing. Journal of Electrochemical Science and Engineering, 14(2), 265–273, 2024. https://doi.org/10.5599/jese.2291.
20. BISTEROV, I.; ABAYZEED, S.; SPEIDEL, A.; CLARE, A. T. On-machine measurement with an electrochemical jet machine tool. International Journal of Machine Tools and Manufacture, 174, 103859, 2022. https://doi.org/10.1016/j.ijmachtools.2022.103859.
21. RAJPUT, Mridul S.; PANDEY, Pulak M.; JHA, Sunil. Experimental investigations into ultrasonic-assisted jet electrodeposition process. **Proceedings of the Institution of Mechanical Engineers, Part B: Journal of Engineering Manufacture**, v. 228, n. 5, p. 682-694, 2014. https://doi.org/10.1177/0954405413506198.
22. XIANG, W.; CHEN, B.; LIU, B.; LIN, C.; YANG, Y. The study of an image feedback-assisted jet electrochemical additive manufacturing process. Journal of Manufacturing Processes, 2025. https://doi.org/10.1016/j.jmapro.2025.09.071.

STATEMENTS AND DECLARATIONS

Funding

The authors would like to thank the National Council for Scientific and Technological Development (CNPq); the Coordination for the Improvement of Higher Education Personnel (CAPES); FINEP (grants 2209/22 and 2127/22); the Minas Gerais State Research Support Foundation (FAPEMIG) (grants APQ-01759-17 and APQ-00403-24); and Equivalent Entity acting as the Basin Agency (ABHA) (grant 003/2024). The authors also acknowledge the FEMEC Maker-UFU funding allocated by the Brazilian National Congress (grants 23117.039298/2021-79 and 23117.024929/2023-17); the Postgraduate Program in Mechanical Engineering (PPGEM-UFU); EMBRAPII-FEMEC-UFU; Finally, the institutional support and technical facilities provided by the FEMEC Maker-UFU Advanced Manufacturing Laboratory, the Electroanalytics Research Center (NuPE-UFU) at the Institute of Chemistry (IQ-UFU), the Laboratory of Tribology and Materials (LTM-UFU), the Laboratory of Scanning Electron Microscopy (LAMEV-UFU), the Multi-User Laboratory Network (RELAM-UFU), the Laboratory for Teaching and Research in Machining (LEPU-UFU), the Center for Research and Development of Welding Processes and Additive Manufacturing (LAPROSOLDA), and the Laboratory of Friction and Wear Technology (LTAD-UFU).

Competing Interests

The authors have no relevant financial or non-financial interests to disclose.

Author Contributions

Thiago Ferreira Querino: [writing, methodology, data processing]. Letícia Bueno do Amaral: [writing, experiments, data processing]. Rafaela Evangelista da Silva: [data processing]. Arthur Alves Fiocchi: [coordination and revision]. All authors read and approved the final manuscript.

Data Availability

The experimental data supporting the findings are available in a repository, or provided as supplementary material, or available from the corresponding author upon reasonable request.

Ethics Approval

Not applicable. This study did not involve human participants or animals.

Consent to Participate

Not applicable.

Consent for Publication

Not applicable. The study does not contain identifiable personal data from human participants.